THERMOCAPILLARY EFFECTS IN LIQUID SYSTEMS OF VARIABLE MASS CONFINED IN A NON-ISOTHERMAL CONTAINER

Mohamed M. El-Gammal[1], Jerzy M. Floryan, Jr[2]
[1] *Postdoctoral Fellow, Mechanical Engineering Department, McMaster University, Ontario, Canada*
[2] *Professor, Mechanical and Materials Engineering Department, The University of Western Ontario, Ontario, Canada*
E-mail: melgamma@gmail.com; mfloryan@eng.uwo.ca

Received March 2006, Accepted September 2010
No. 06-CSME-14, E.I.C. Accession 2933

ABSTRACT

Interface deformation and thermocapillary rupture in a non-isothermal cavity with free upper surface is investigated. Temperature variations along the interface are induced by differentially heated walls. The dynamics of the process is modulated by changing mass of the liquid. The results determined for the large Biot and zero Marangoni numbers show the existence of limit points beyond processes leading to the interface rupture set in. Evolution of the limit point as a function of the liquid mass is investigated. The topology of the flow field is very similar regardless of whether the cavity is over-filled or only partially filled. It is shown that the cavity over-filling may, in general, extend the range of admissible capillary numbers and thus it can be used as a tool for prevention of rupture.

Keywords: thermocapillary convection; liquid interfaces; containerless materials processing.

EFFETS THERMOCAPILLAIRES DANS DES SYSTÈMES LIQUIDES DE MASSE VARIABLE CONFINÉS DANS UN CONTENANT NON ISOTHERME

RÉSUMÉ

Cet article s'intéresse à la déformation d'interface et à la rupture thermocapillaire dans une cavité non isotherme à surface supérieure libre. Les variations de température le long de l'interface sont induites par des parois chauffantes différentielles. La dynamique du procédé est modulée en changeant la masse du liquide. Les résultats déterminés pour les nombres Biot et Marangoni démontrent l'existence de points limites au-delà des procédés menant à la rupture de l'interface. L'évolution du point limite comme fonction de la masse liquide est étudiée. La topologie du champ d'écoulement est très semblable sans égard au fait que le remplissage de la cavité est excessif ou partiel. Il est démontré que le remplissage excessif peut, en général, étendre la mesure des nombres de capillarité admissibles et ainsi pourrait être utilisée pour prévenir la rupture.

Mots-clés : convection thermocapillaire; interfaces des liquides; traitement des matériaux sans contenant.

1. INTRODUCTION

Thermocapillary effects give rise to various phenomena arising at differentially heated liquid interfaces. These phenomena include convective flows as well as interface distortions, including interface rupture. Convective flows and the associated instabilities have been subjected to numerous investigations [1–5] while the analysis of interface deformation and possible rupture has attracted attention more recently [6]. Interfacial effects are important in many technical processes where they can play a dominant role, e.g., zero-gravity containerless materials processing, or could represent a contributing factor, e.g., coating flows in semiconductor processing, manufacturing of digital storage media, disperse phase micro-reactors, dynamics of foams and emulsions, microfluidics, enhanced oil production, conventional crystal growth, dynamics of welds, chemically driven flows, etc. Control and optimisation of these processes critically depend on the complete understanding of liquid response driven by surface tension effects, including the thermocapillary effect. The focus of the present work is on studying thermocapillary flows in the absence of any body force or when the body forces, like gravity, play a negligible role.

Thermocapillary flows are driven by the imbalance of the tangential stress on the interface caused by temperature dependence of surface tension [7]. The character of the response of the liquid depends on the temperature distribution along the interface, and thus it depends in general on the overall heat transport in the flow system. This temperature can be predicted only in special situations, such as heat transfer dominated by conduction in one of the phases. Additional complications arise due to possible variations of geometry of the container and a wide range of possible heating strategies. In the geometrically simplest case of liquid contained in a rectangular cavity open from above, the heating can be applied either through the bottom, or through the sidewalls, or from above, and could have various spatial distributions. The dynamics of the system is remarkable different in each of these cases even for the simplest forms of heating.

The simplest case of heating through the cavity bottom involves liquid with initially flat interface resting on an isothermal, flat, solid plate. The resulting temperature field gives rise to the temperature gradient vector that is normal to the interface at the interface. The liquid motion can be induced through an instability process first studied by Pearson [8]; this process is usually referred to as the Marangoni instability. There are two instability mechanisms possible. The first one relies on convective effects and Pearson [8] determined the relevant critical conditions. The second one relies on the interface deformation; Czechowski and Floryan [9] established the critical conditions relevant to this case. When the cavity is sufficiently long, the second mechanism dominates, resulting in an unconditional instability that initiates processes leading to rupture of the interface [9].

When the liquid is heated through the sidewalls, such as in the case of horizontal direct crystallization [10], the resulting temperature gradient has a component in the direction parallel to the interface. In this case the thermocapillary effect always generates some motion, regardless of the magnitude of temperature gradient. Floryan and Chen [11] showed that a long continuous liquid layer exposed to such heating may exist only when the temperature field satisfies restrictive existence conditions. The explicit form of these conditions, determined for the case of negligible convective transport, demonstrates that the required temperature fields are rather unusual and are unlikely to be encountered in practice, and thus interface deformation is expected to play the dominant role in the system response. The long liquid layers cannot be realized in practice under non-isothermal conditions and thus one need to focus on the analysis of the interface rupture and the topology of the resulting liquid masses. Kurosawa et al. [11] showed experimentally that large interface deformations do occur in long liquid layers if the level of gravity is sufficiently reduced.

The simplest form of the heating through the sidewalls corresponds to the conduction-dominated heat transfer in the gas phase resulting in the linear temperature distribution along the interface. This particular type of heating has been widely studied and represents a convenient reference case [12]. Laure et al. [13] and Ben Hadid and Roux [14] described the differences in the flow patterns at the cold and hot ends of long cavities with non-deformable interface at higher values of Reynolds numbers. Canright and Huber [15] analysed in detail flow structure at the cold corner. Zebib et al. [16] and Carpenter and Homsy [17] investigated the formation of boundary layers in a square cavity with a fixed interface at high values of Reynolds numbers. Torii [18] investigated unsteady effects. Liu et al. [19] modelled encapsulation effect and considered system made of two fluid layers. Braverman et al. [20] investigated anomalous thermocapillary effect. Peltier and Biringen [21] used direct numerical simulation in studying the transition between steady and time dependent convections. Chen and Hwu [22] included effects of interface deformability and concluded that instability may occur at a Marangoni number considerably lower than the one found in the case of a non-deformable interface. Hamed and Floryan [23] showed that large interfacial deformations might occur, leading to rupture of the interface through formation of dry spots at the sidewalls if the contact points are fixed. Jiang et al. [24] demonstrated similar phenomena in the case of fixed contact angles constraint, with rupture leading to the formation of dry spots at the cavity bottom. They determined location of the limit points in the parameter space beyond which a steady, continuous interface cannot exist [23,24]. Jiang and Floryan [25] demonstrated that insulating interface could increase deformation.

An up-to-date review of experimental investigation has been given by Schatz and Neitzel [3] and will not be repeated here. Recent experiments of Benz and Schwabe [26] show an interesting dependence of convection patterns on the level of gravity under conditions where nominally thermocapillary effect should dominate.

All available analyses have been carried out with the interface being initially flat. It is not known how the system response may change when the cavity is either over-filled or only partially filled. The initial shape of the interface is of particular importance in experiments where special precautions need to be taken in order to overcome meniscus effect and produce flat interface. This process is simplified in the case of terrestrial experiments where the experimentalist is assisted by hydrostatic pressure, but remains a concern in the case of well-controlled space experiments.

The present study is focussed on the analysis of the dynamics of the liquid when the isothermal interface assumes an arbitrary form. The permissible forms are described by the Young-Laplace equation. The temperature gradient along the interface is created through differential heating of the sidewalls. Two cases of dynamical response are considered. The first one corresponds to the interface being subject to the fixed contact point constraint and the second one corresponds to the fixed angles constraint. The fixed contact angles condition represents the real case for thermocapillary flows inside rectangular cavities. However, to reduce the surface deformation and thus extend the range of admissible capillary numbers, fixed contact points interface condition is sought. The location of the contact points can be fixed in an actual experiment by attaching two small wedges to the side walls at the upper cavity ends.

In all cases considered, the initial form of the constraint, i.e., either the initial locations of the contact points or the initial contact angles, is preserved during the heating. El-Gammal et al. [27] suggested that cavity overfilling can be used for control of interface rupture. The present paper provides a detailed analysis of this problem. Since the governing equations are not amenable to analytical, we shall rely on numerical simulations.

The paper is organized as follows. Section 2 gives the formulation and explains the notation used. Section 3 is devoted to the discussion of our results. Section 4 gives a short summary of the main conclusions.

2. PROBLEM FORMULATION

Consider liquid in a cavity of length L, as shown in Fig. 1. The cavity, which is open from above, is formed by isothermal solid walls on the left and right sides, and by an insulated solid plate on the bottom. The liquid is incompressible, Newtonian, has density ρ, thermal conductivity k, specific heat per unit mass c, thermal diffusivity $\kappa = k / \rho c$, kinematic viscosity ν and dynamic viscosity μ. The free surface, described by $y = h(x)$, is bounded by a passive gas of negligible density and viscosity. This free surface is associated with a surface tension σ, which is a function of the local temperature. It is assumed, without loss of generality, that the pressure in the gas phase is negligible.

The isothermal interface is described by the Laplace-Young equation whose solution in the case of an interface passing through the contact points at $(x,y)=(\pm L/2, H)$ has the form

$$h_0(x) = D + H + D|D|^{-1}\left[-R + \left(R^2 - x^2\right)^{1/2}\right], \quad R = \left(L^2/4 + D^2\right)|D| / \left(2D^2\right) \tag{1}$$

where R denotes the radius of curvature of the interface and D stands for the bulge factor, whose positive values correspond to the interface bulging out (see Fig. 1).

When the cavity sidewalls are differentially heated, thermocapillary effect acting along the interface gives rise to convection. The steady, two-dimensional convection is governed by the continuity, Navier-Stokes and energy equations subject to the following boundary conditions:

$$x = L/2: \qquad \mathbf{U} = 0, \ T = T_R, \tag{2a}$$

$$x = -L/2: \qquad \mathbf{U} = 0, \ T = T_L, \tag{2b}$$

$$y = 0: \qquad \mathbf{U} = 0, \ T_y = 0, \tag{2c}$$

$$F(x,y) = y - h(x) = 0: \quad \mathbf{U}\cdot\nabla\mathbf{F} = 0, \ \mathbf{S}\cdot\mathbf{n} = 2\sigma\Lambda\mathbf{n} + \sigma_s\mathbf{t}, \ k\nabla\mathbf{T}\cdot\mathbf{n} + h_g\left(T - T_g\right) = 0 \tag{2d - f}$$

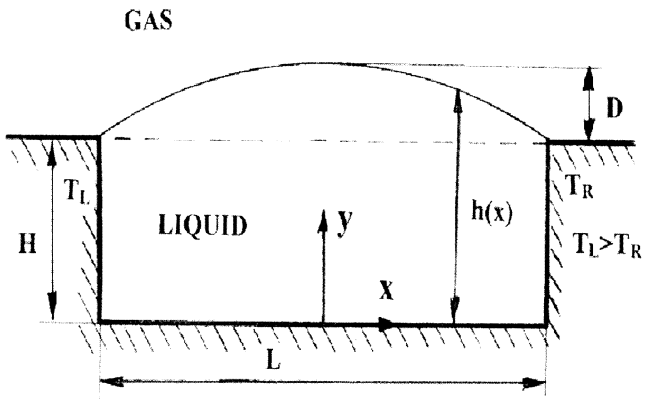

Fig. 1. Sketch of the flow model problem.

In the above, $\mathbf{U}= u\,\mathbf{i} + v\,\mathbf{j}$ is the velocity vector, $\mathbf{i}$ and $\mathbf{j}$ are the unit vectors in the x- and y-directions, respectively, T is the temperature of the liquid, S is the stress tensor in the liquid, Λ stands for the mean curvature of the interface, ∇ denotes the nabla operator, $\mathbf{n}$ stands for the unit vector normal to the interface pointing outwards, $\mathbf{t}$ denotes the unit vector tangential to the interface, and the subscripts n, s denote normal and tangential derivatives at the interface, respectively.

Equations (2a–c) describe the no-slip and no-penetration conditions at the solid walls. Eq. (2d) is the kinematic condition at the liquid-gas interface. The stress balances at the interface are given by (2e). The jump in the normal stress across the interface is balanced by the surface tension times the mean curvature, and the jump in the shear stress at the interface is balanced by the surface tension gradient. The unit vectors are defined as follows $\mathbf{n}=(-h_x\mathbf{i}+\mathbf{j})/N$, $\mathbf{t}=(\mathbf{i}+h_x\mathbf{j})/N$, where $N=(1+h_x^2)^{1/2}$. The mean curvature Λ of the interface in (2e) has the definition $\Lambda=-\nabla\cdot\mathbf{n}/2=h_{xx}N^{-3}/2$. The thermal boundary condition at the interface is given by (2f) in which k is the thermal conductivity of the liquid, h_g is the heat transfer coefficient in the gas and $T_g(x)$ is the temperature in the gas phase.

The thermal boundary condition (2f) presumes that the $T_g(x)$ is known and that the heat transport at the liquid-gas interface can be described by using a heat-transfer coefficient h_g. It is assumed in the present analysis that the liquid is subject to a heating through the cavity sidewalls, which are maintained at constant temperatures T_L and T_R, and that the heat transport in the gas phase is dominated by conduction, which leads to a linear temperature distribution in the gas phase along the interface. It is further assumed that the heating of the sidewalls is a function of cavity length and is adjusted in such a way that the temperature gradient along the interface is constant regardless of the cavity length L, i.e., $T_g(x)=-(T_L-T_R)L^{-1}x + (T_L+T_R)/2$.

Apart from boundary conditions (2a–f), the liquid must also satisfy the mass conservation constraint. Since the liquid is assumed to be incompressible, its total volume must remain constant, i.e.

$$\int_{-L/2}^{L/2} h(x)dx = V \tag{2g}$$

where $V=\left(H+D-DR|D|^{-1}\right)L+D|D|^{-1}\left[L\left(R^2-L^2/4\right)^{1/2}+2R^2\arcsin(L/(2R))\right]\Big/2$. The problem is closed by specifying the type of contact made by the interface at the sidewalls. Here, we shall consider two cases, i.e., an interface with fixed contact points

$$x=\pm L/2:\ h=H, \tag{2h}$$

and an interface sliding along the sidewalls with a fixed contact angle equal to the isothermal contact angle

$$x=\pm L/2:\quad h_x=-D|D|^{-1}x\left(R^2-x^2\right)^{-1/2}. \tag{2i}$$

We shall use a linear equation of state for surface tension. In particular, we take $\sigma(T)=\sigma^*-\gamma(T-T^*)$, where σ^* is the surface tension of the liquid at the reference temperature $T^*=(T_L+T_R)/2$ and the constant γ is the negative of the derivative of the surface tension with

respect to temperature. We scale the problem using H as the length scale, u^* as the velocity scale, $\mu u^*/H$ as the pressure scale and σ^* as the surface tension scale. The dimensionless temperature T' is defined as $T - T^* = \Delta T\, T'$, where $\Delta T=(T_L-T_R)H/L$. The gas temperature is scaled in a similar manner leading to $T_g'=-x$. The characteristic velocity u^* is derived from the so-called Marangoni effect, i.e. the jump in the shear along the interface balances the surface tension gradient, which results in $u^*=\gamma\Delta T/\mu$. With the above definitions, the dimensionless equations (with primes dropped) can be written in the form

$$u_x + v_y = 0, \quad Re\left(uu_x + vu_y\right) = -p_x + u_{xx} + u_{yy}, \tag{3a - b}$$

$$Re\left(uv_x + vv_y\right) = -p_y + v_{xx} + v_{yy}, \quad Ma\left(u\,T_x + v\,T_y\right) = T_{xx} + T_{yy}. \tag{3c - d}$$

where p denotes pressure. The Reynolds number Re and the Marangoni number Ma are defined as $Re=u^*H/\nu$ and $Ma=u^*H/\kappa$, respectively. The boundary conditions and constraints transform to

$$x=-L/2 : u=v=0,\ T=L/2,\ h=1 \text{ or } h_x=-D|D|^{-1}L\left(R^2-L^2/4\right)^{-1/2} \tag{4a}$$

$$x=L/2 :\ u=v=0,\ T=-L/2,\ h=1 \ \text{ or } \ h_x=-D|D|^{-1}L\left(R^2-L^2/4\right)^{-1/2}, \tag{4b}$$

$$y=0 : u=v=\ T_y=0, \tag{4c}$$

$$y=h(x) : uh_x-v=0, \tag{4d}$$

$$-p+2\left[v_y-h_xu_y+h_x(-v_x+h_xu_x)\right]\left(1+h_x^2\right)^{-1}=Ca^{-1}(1-CaT)h_{xx}\left(1+h_x^2\right)^{-3/2} \tag{4e}$$

$$2h_x\left(-u_x+v_y\right)+\left(1-h_x^2\right)\left(v_x+u_y\right)=-\left(T_x+h_xT_y\right)\left(1+h_x^2\right)^{1/2} \tag{4f}$$

$$\left(-h_xT_x+T_y\right)\left(1+h_x^2\right)^{-1/2}+Bi(T+x)=0, \ \int_{-L/2}^{L/2} h(x)dx=V. \tag{4g - h}$$

In the above, (4d) is the kinematic condition, (4e) and (4f) are the stress balances in the normal and tangential directions, respectively, and (4g) describes the heat transfer condition. In (4e) Ca is the capillary number, given by $Ca=\mu u^*/\sigma^*=\gamma\Delta T/\sigma^*$. The Biot number Bi in (4g) is defined as $Bi = h_gH/k$ and measures the heat transport between the gas and the liquid phase.

The flow problem (3–4) has to be solved on an irregular solution domain whose shape is determined by the unknown location of the free surface h(x). The numerical solution relies on a

finite-difference discretization. The required regularization of the solution domain is achieved by mapping the physical domain onto a computational domain using transformation $\xi=x$, $\eta=y/h(x)$. The mapping in the y-direction fixes the computational domain in $\eta\in(0,1)$. Chen and Floryan [28] developed the relevant algorithm and its description is omitted from this presentation. Hamed and Floryan [29] provided extension of this algorithm to time-dependent situations. A rectangular computational grid of size $\Delta\xi$, $\Delta\eta$ in the ξ,η directions is used, with grid lines parallel to the ξ and η axes and such that the grid fits exactly the geometry of the computational domain, with the side and bottom walls and the interface as certain grid lines. The accuracy of the numerical solution depends on the grid structure used during computations. The maximum acceptable grid size has been determined using grid convergence studies. It has been found that flows with the largest values of Re, D and Ca were the most demanding in terms of accuracy. Table 1 illustrates results of tests and grids selected for computations that provide accuracy no worse then 2% for the location of the interface. The tests have been carried out for the extreme values of the parameters considered in this study and, in particular, for values of Ca that are very close to the limit point of the system.

Table 1. Results of grid convergence studies for the interface subject to the fixed contact point constraint for cavity length L=6. Grids shown in italics have been selected for the computations.

	Grid spacing		
Test conditions	$\Delta\eta$	$\Delta\xi$	Deformation $\lvert h(x)-h_0(x)\rvert$
Re=1,	*1/20*	*1/120*	0.40896
D=0.5,	1/40	1/120	0.40793
Ca=0.2,	1/20	1/240	0.40895
x=-2.5			
Re=1,	*1/20*	*1/120*	0.39751
D=0,	1/40	1/120	0.39667
Ca=0.13,	1/20	1/240	0.39784
x=-2.5			
Re=1,	*1/20*	*1/120*	0.26551
D=-0.5,	1/40	1/120	0.26520
Ca=0.05,	1/20	1/240	0.26608
x=-2.5			
Re=400,	1/60	1/120	0.13339
D=0.5,	*1/80*	*1/120*	0.13528
Ca=0.3,	1/140	1/120	0.13664
x=-2	1/80	1/240	0.13634
Re=400,	1/60	1/120	0.33936
D=0,	*1/80*	*1/120*	0.33340
Ca=0.21,	1/100	1/120	0.33137
x=-2.5	1/80	1/240	0.33147
Re=400,	1/20	1/120	0.36816
D=-0.5,	*1/40*	*1/120*	0.35377
Ca=0.07,	1/60	1/120	0.35122
x=-2.5	1/80	1/240	0.35081

3. DISCUSSION OF RESULTS

We shall investigate the behaviour of the liquid contained in the cavity shown in Fig. 1. In order to simplify discussion, we shall only consider the conduction limit Ma $\rightarrow$ 0 and large Biot number limit Bi $\rightarrow \infty$. The first condition limits our results to highly conductive liquids ($k \rightarrow \infty$) such as liquid metals. The second condition implies a very high heat transfer coefficient in the gas phase at the interface, which makes the temperature of the interface effectively equal to the temperature of the gas phase. We select cavity length L=6 for our discussion as the response of the system with such length with interface initially flat is well documented [23,24].

3.1.1 The Fixed Contact Points Case

Figure 2a illustrates flow patterns in the cavity that is initially over-filled with the liquid for Re=1 and for two extreme values of capillary number permitted. The reader may note that increasing Ca corresponds to the interface becoming progressively softer. Figure 2a shows flow for Ca=0.02 when the interface deformation is fairly small. The flow is driven along the interface from the hot wall to the cold wall and is forced to move back along the bottom of the cavity in order to conserve mass, producing a very large re-circulating vortex filling the interior of the flow domain. There are additional vortices at the bottom corners (not shown in the plots) whose structure have been described by Moffat [30] and thus will not be discussed here. There are no vortices around the upper corners, as shown by Anderson and Davis [31]. The return motion is driven by the longitudinal pressure gradient, which generates most of the interface deformation. The interface slightly rises up at the cold side and recedes at the hot side.

When capillary number increases, the interfacial distortion increases as illustrated in Fig. 2a for Ca=0.2. This value of Ca represents a near maximum value permitted for the flow conditions being discussed. The vortex core moves into the ''bulge'' forming at the cold side. The shape of the interface suggests eventual rupture and formation of a dry spot at the hot wall.

Figure 2b displays flow patterns in the case of the cavity completely filled with the liquid and the interface being initially flat for the same value of Re=1. The flow pattern is qualitatively similar as in the case of the over-filled cavity, with the velocity of motion reduced due to the constraint imposed by the smaller depth of the liquid. The deformation pattern is also similar, with the magnitudes being larger due to the larger pressure gradients required to produce the return motion. Figure 2c displays patterns in the case partially filled cavity for Re=1, with the interface reaching initially half cavity depth. The flow pattern consists now of two distinct vortex cores surrounded by the liquid flowing around them; some of the liquid becomes permanently trapped inside these cores. The magnitude of the velocity significantly decreases due to the increased resistance associated with the small depth of the liquid. As deformation increases, the intensity of the motion in the vortex at the hot side noticeably decreases due to the increase of friction associated with the reduction of the available flow area. The magnitude of the deformation increases, as the pressure difference required to produce the back flow is now much bigger.

The interplay between the cavity over-fill and the resulting interface deformation is illustrated in Fig. 3 for the same value of Re, i.e., Re=1. This figure shows variations of the maximum deformation defined as $\max|h_f\text{-}h_0|$, where h_f denotes the final shape of the interface and h_0 denotes the initial (isothermal) shape of the interface, as a function of capillary number Ca. The forms of these curves show that when Ca increases the amplitude of the deformation increases at a rapidly accelerating rate. It is clear that when Ca reaches a certain critical value a continuous, steady interface connecting contact points cannot exist. This value of $Ca = Ca_{cr}$

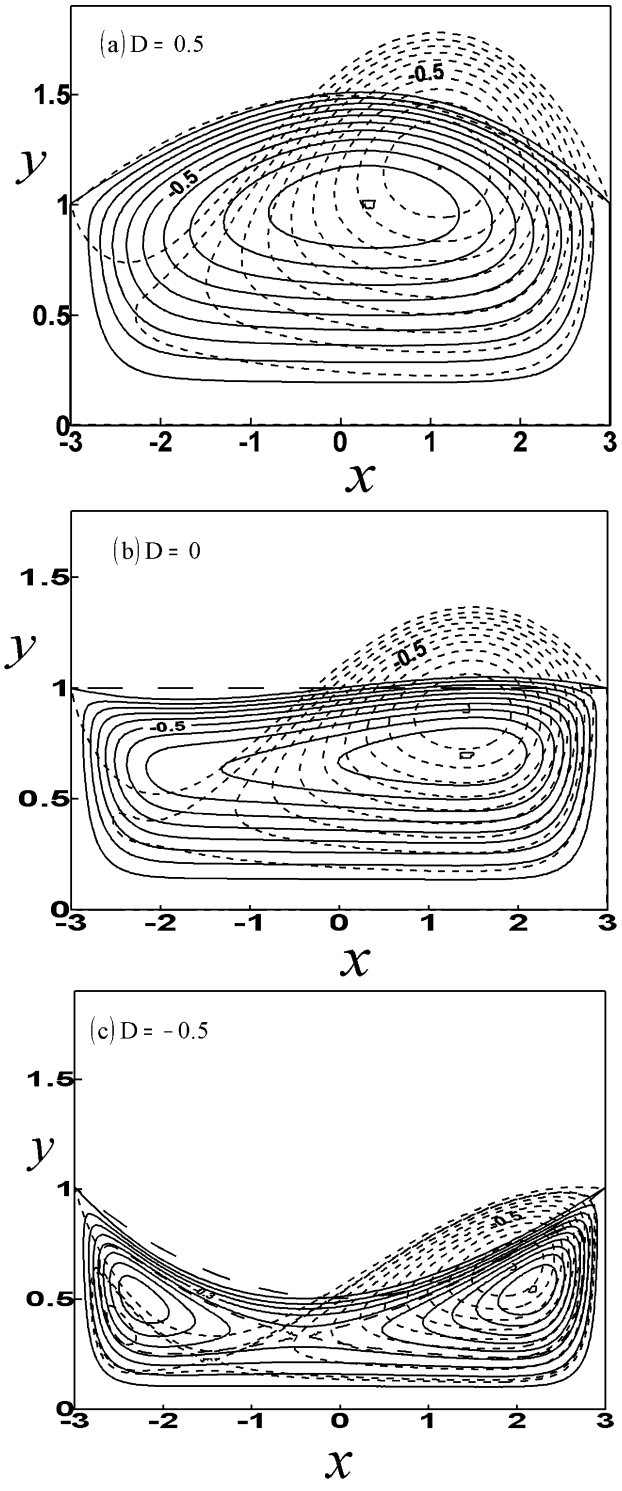

Fig. 2. Flow patterns for Re=1 and the interface subject to the fixed contact points constraint. Contour lines are shown every 10% of ψ_{max}. Long-dash lines shows isothermal interface. Figure 2a–D=0.5: solid lines - Ca=0.02, $|\psi_{max}|$=0.0907; dash lines – Ca=0.2, $|\psi_{max}|$=0.1466. Figure 2b–D=0: solid lines - Ca=0.02, $|\psi_{max}|$=0.0411; dash lines – Ca=0.13, $|\psi_{max}|$=0.0803. Figure 2c–D=−0.5: solid lines - Ca=0.01, $|\psi_{max}|$;=0.0205; dash lines – Ca=0.05, $|\psi_{max}|$=0.0338.

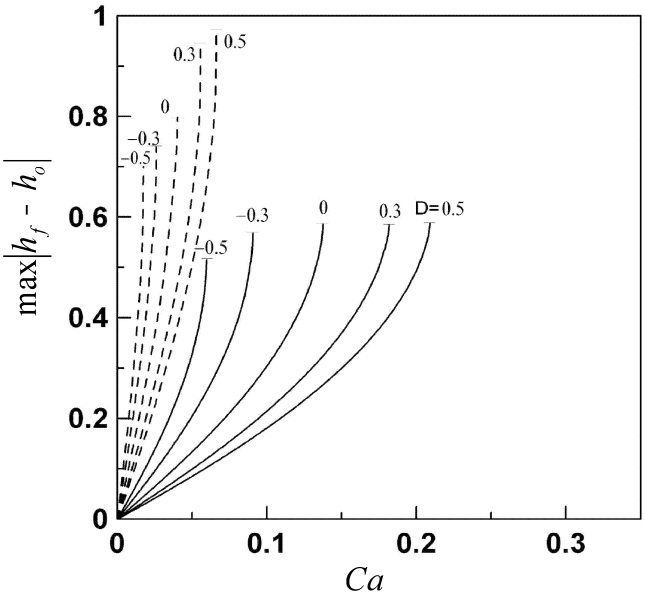

Fig. 3. The maximum interface deformation as a function of capillary number Ca for different values of the bulge factor D and for Re=1. Continuous and dash lines describe the fixed contact points and the fixed contact angles cases, respectively.

defines the limit point for the system. It was shown by Hamed and Floryan [23] that deformation increases continuously in time for $Ca>Ca_{cr}$ without reaching a saturation state in the case of mass of the liquid such that the cavity is completely filled. It can be seen that the rate of approach to the limit point increases as the amount of the liquid in the cavity is reduced. The permissible capillary number that guarantees the existence of a continuous interface more than doubles when the amount of the liquid, as measured by the bulge factor D, is increased from $D=-0.5$ to $D=0.5$.

Figure 4 illustrates the evolution of the surface pressure and the shape of the interface as a function of Ca for three levels of the cavity over-fill for Re=1. The characteristic bulging of the interface at the cold side, increasing with an increase of Ca, can be clearly seen in all cases. Surface pressure variations for the over-filled cavity (Fig. 4a) suggest the existence of a core zone away from the sidewalls where the pressure gradient is almost constant and the flow is very similar to the Couette-Poiseuille flow with zero mass flux, as in the case of cavity with fixed interface [12]. This similarity exists even in the case of the largest possible deformation. One should note that as the magnitude of the deformation increases, the lengths of the turning zones increase; this effect is more pronounced at the hot wall than at the cold wall (see Fig. 4a). The pressure peaks around both walls are consistent with the analytical predictions given by Anderson and Davis [31]. The lack of symmetry between the cold and hot end circulations has already been identified previously in the case of flat non-deformable [13,14] and deformable interfaces [23] and is well demonstrated in the present case. When the mass of the liquid is reduced (D=0, Fig. 4b), the decrease in the depth results in an increased viscous resistance. This leads to a larger pressure gradient that needs to be generated in order to generate the back flow (compare Figs. 4a and 4b) and thus increased interface deformation. The spatial constraints associated with the reduced amount of liquid result in longer turning zones, especially at higher values of Ca (see Fig. 4b). This process is more pronounced with the further reduction of the mass of the liquid, as illustrated in Fig. 4c for $D=-0.5$. The pressure gradient is now much

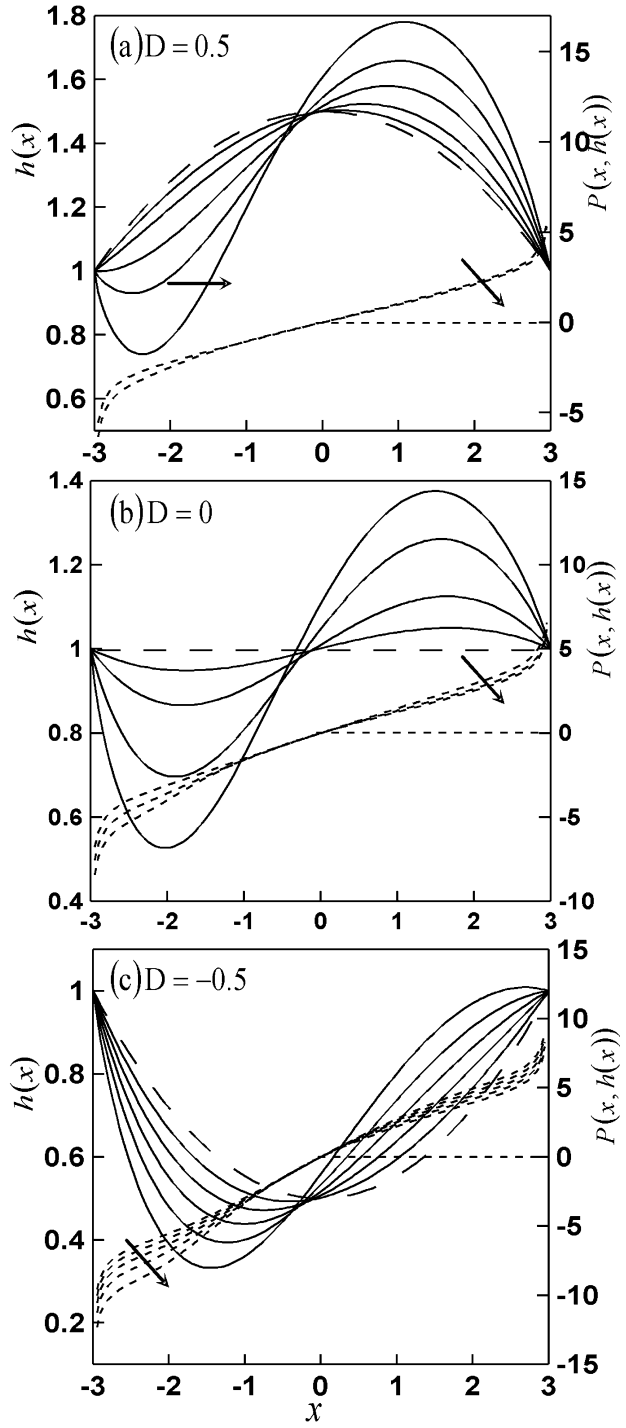

Fig. 4. The evolution of the surface pressure and the shape of the interface as a function of capillary number Ca for Re=1 and the interface subject to the fixed contact points constraint. Figure 4a–D=0.5 (interface shown for Ca= 0.02, 0.05, 0.1, 0.15, 0.2; pressure shown for Ca=0.02, 0.2); Figure 4b–D=0 (interface shown for Ca=0.02, 0.05, 0.1, 0.13; pressure shown for Ca= 0.02, 0.1, 0.13); Figure 4c –D=−0.5 (interface and pressure shown for Ca= 0.01, 0.02, 0.03, 0.04, 0.05). The long-dash line shows isothermal interface. The top dash line always corresponds to the pressure with the lowest Ca.

bigger, the size of the core zone is significantly reduced and the turning zones occupy more than 2/3 of the cavity length. The pressure distribution in the turning zones changes significantly as Ca increases, primarily due to the spatial constraint imposed on the flow by the form of the interface. The reader may also note a significant increase of differences between circulations at both ends of the cavity.

Figure 5a displays flow patterns when Reynolds number increases to Re=400 and the cavity is initially over-filled resulting in the bulge factor D=0.5. The flow pattern is qualitatively similar as in the case of small Re (compare Figs. 2a and 5a), with the vortex centre moved significantly closer to the cold wall. Because of the magnitude of Re the vortex acquires inviscid characteristics (with approximately constant vorticity in its interior) and its structure closely resembles the Batchelor's model [32] for steady laminar flow with closed streamlines at large Re. The deformation pattern acquires special features, especially at higher values of Ca. Because of large depth of the liquid and high value of Re the pressure difference required to generate the back flow is fairly small. Additional pressure variations are imposed by the action of the vortex whose presence is responsible for the local reduction of the surface pressure and the resulting "depression" in the surface elevation above it. Because the local pressure drop associated with the action of the vortex is so large, the resulting "depression" in the shape of the interface is sufficiently large to force the interface to recede at the cold side and rise up at the hot side, which is opposite to what has been observed at low values of Re. We shall return to this question during discussion of pressure variations. It is of interest to note the formation of a small bulge at the vicinity of the cold wall as Ca increases, which suggests that processes leading to the formation of the limit point will be driven by the dynamics around the cold corner, with the elevation of the contact point likely increasing and with no danger of formation of a dry spot.

Figure 5b illustrates flow patterns in the cavity initially completely filled with the liquid with D=0 for the same value of Re=400. The depth of the liquid is smaller as compared to the case discussed above, which leads to an increased friction and reduced magnitude of velocity. Vortex generates local pressure reduction, although the "dip" in the interface is smaller as compared to the case of the over-filled cavity (compare Figs. 5a and 5b). The deformation pattern returns to the form observed in the case of small Re (compare Figs. 2b and 5b). Figure 5c illustrates flow patterns in the case of a partially filled cavity for the same value of Re. There are two vortex cores when Ca is sufficiently small. Increase of Ca leads to a higher deformation and pronounced dominance of the vortex core at the cold side. The deformation pattern is very similar as in the case of Re=1 (compare Figs. 2c and 5c). The interface does not appear to be affected by the local pressure reduction associated with the presence of the vortex. The form of the interface suggests eventual rupture and formation of a dry spot at the hot wall.

The interplay between the cavity over-fill and the resulting interface deformation in the case of Re=400 is illustrated in Fig. 6 displaying the maximum deformation $\max|h_f-h_0|$ as a function of capillary number Ca. It is clear that when Ca reaches a certain critical value a continuous, steady interface connecting contact points cannot exist. It can be seen that the rate of approach to the limit point increases as the amount of the liquid in the cavity is reduced. The permissible capillary number that guarantees the existence of a continuous interface more the triples when the amount of liquid as measured by the bulge factor is increased from D=−0.5 to D=0.5. Comparison with the case of small Re (Fig. 3) demonstrates that an increase of Re reduces the magnitude of the deformation for all levels of cavity over-fill and significantly expands the range of permissible capillary numbers. This increase is more pronounced in the case of the over-filled cavities as compared to the partially filled cavities.

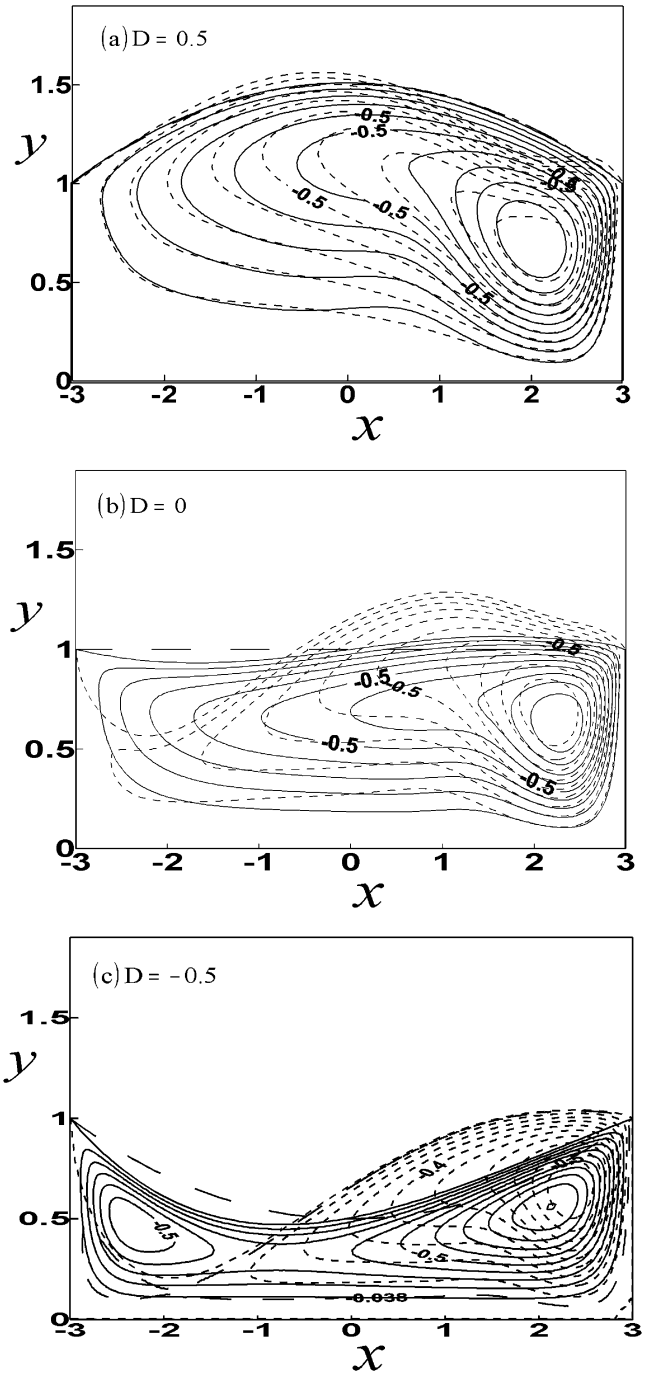

Fig. 5. Flow patterns for Re=400 and the interface subject to the fixed contact points constraint. Contour lines are shown every 10% of ψ_{max}. Long-dash lines shows isothermal interface. Figure 5a–D=0.5: solid lines - Ca=0.02, $|\psi_{max}|$=0.0637; dash lines – Ca=0.31, $|\psi_{max}|$=0.0597. Figure 5b–D=0: solid lines - Ca=0.05, $|\psi_{max}|$=0.0455; dash lines – Ca=0.2, $|\psi_{max}|$=0.0538. Figure 5c–D=-0.5: solid lines - Ca=0.02, $|\psi_{max}|$=0.0230; dash lines – Ca=0.0708, $|\psi_{max}|$=0.0334.

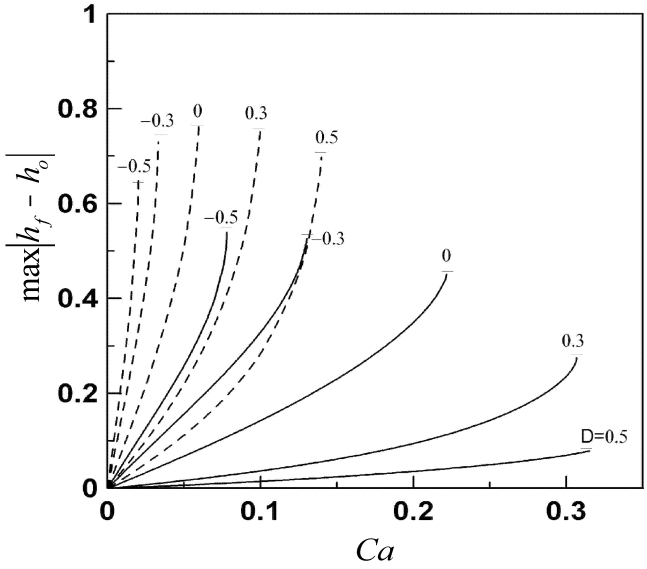

Fig. 6. The maximum interface deformation as a function of capillary number Ca for different values of the bulge factor D and for L=6, Re=400. Continuous and dash lines describe the fixed contact points and the fixed contact angles cases, respectively.

Figure 7 illustrates the evolution of the surface pressure and the shape of the interface as a function of Ca for Re=400 for the same levels of the cavity over-fill as discussed above. There are two patterns of interface deformation, one with the interface receding at the cold end (Fig. 7a) and one with the interface rising up at the cold end (Figs. 7b,c). We shall begin our discussion with the former case. The turning zone at the hot end is very small for D=0.5 as shown in Fig. 7a. The core zone is moved to the left and the pressure gradient producing the back flow is very small. Vortex activity at the right side produces local pressure drop and a very large ''dip'' in the interface elevation. This ''dip'' increases as Ca increases resulting in the interface rising up at the hot side. The overall deformation pattern is dominated by the vortex effect. A very large local pressure rise at the cold end is associated with the interaction between the vortex and the sidewall [15,30]. When the mass of the liquid is reduced to D=0 (Fig. 7b), the depth of the liquid decreases, the intensity of the vortex decreases, the local pressure drop associated with the vortex decreases, the length of the core zone decreases, the pressure gradient in the core zone increases, and the lengths of the turning zones increase. The overall deformation pattern changes with the interface rising up at the cold end. The deformation is dominated by the pressure gradient associated with the back flow, and not by the vortex effect as in the previous case. The resulting magnitude of interface deformation is significantly larger and its form suggests eventual formation of a dry spot at the hot wall for sufficiently large Ca. The same trend continues with the further reduction of the mass of liquid. In the case of D=−0.5 (Fig. 7c), the core zone is difficult to identify, the average pressure gradient is much bigger, the pressure distribution in the turning zones changes significantly as a function of Ca, the local pressure reduction associated with the vortex is further reduced and is unable to produce any noticeable ''dip'' in the shape of the interface. The magnitude of the deformation, which is dominated by the pressure gradient, is significantly higher as compared to the case of D=0 (compare Figs. 7b–c).

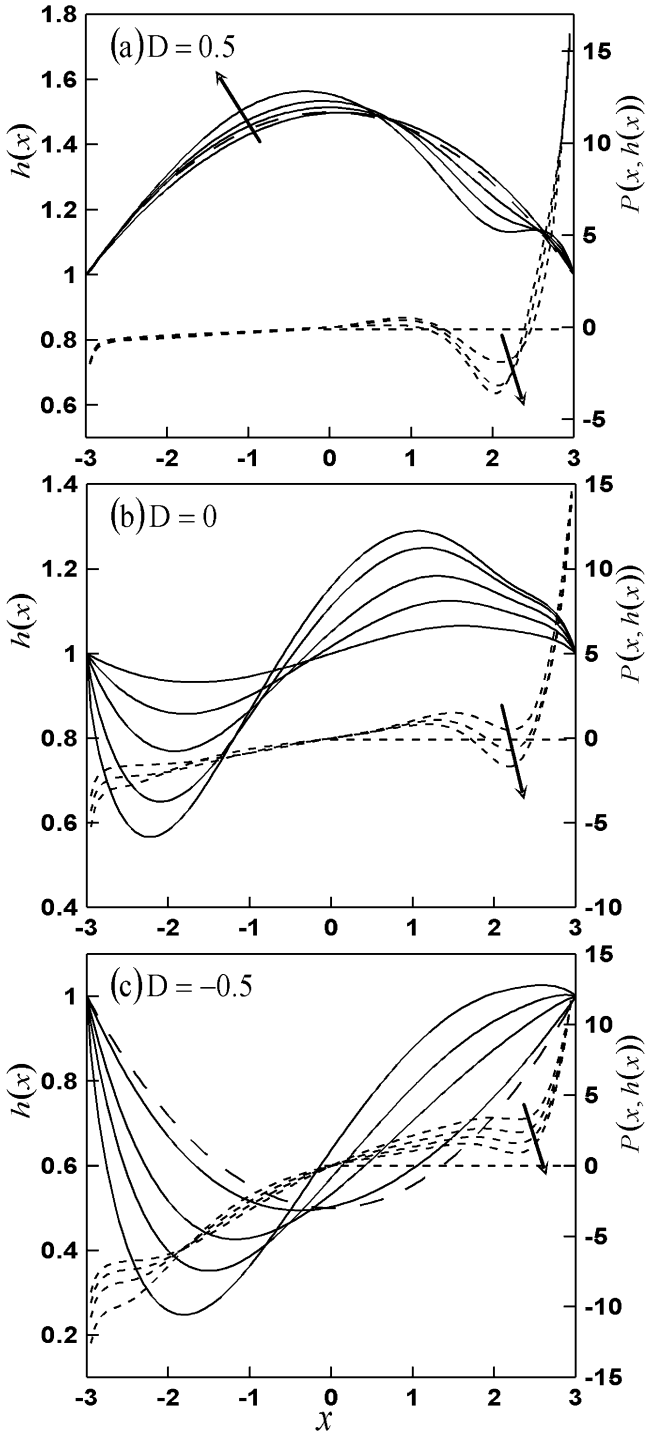

Fig. 7. The evolution of the surface pressure and the shape of the interface as a function of capillary number Ca for Re=400 and the interface subject to the fixed contact points constraint. Figure 7a– D=0.5 (interface shown for Ca=0.02, 0.1, 0.2, 0.31; pressure shown for Ca=0.02, 0.2, 0.31); Figure 7b– D=0 (interface shown for Ca=0.05, 0.1, 0.15, 0.2, 0.22; pressure shown for Ca=0.05, 0.15, 0.22); Figure 7c –D=-0.5 (interface and pressure shown for Ca=0.02, 0.04, 0.06, 0.0708). The long-dash line shows isothermal interface. The top dash line always corresponds to the pressure with the lowest Ca.

3.1.2 The Fixed Contact Angles Case

The wetting conditions permit the contact points to move during the heating, with the contact angles being fixed and equal to their isothermal values. We investigate the final state of the system when the contact points have already reached their final destination. We assume that the sidewalls are high enough to prevent liquid from spilling out of the cavity.

Figure 8a illustrates the flow pattern in a cavity with D=0.5 for Re=1 and for two extreme values of Ca. The reader may note that Ca=0.06 (see Fig. 8a) represents a near maximum permitted value for these flow conditions. The topology of the flow is similar to the case with the fixed contact points (compare Figs. 2a and 8a), i.e., it consists of a large re-circulating vortex driven along the interface from the hot to the cold end and a backflow along the bottom forced by the pressure gradient, and corner vortices (not shown). The deformation pattern is qualitatively similar in the sense that it is dominated by the pressure gradient with the interface moving up at the cold end. The actual shape of the distorted interface is very much different (compare Figs. 2a and 8a) as the end points are permitted to move during the heating. This shape suggests eventual formation of a dry spot at the cavity bottom on the hot side. The magnitude of the deformation is significantly larger than in the case of fixed contact points and thus the interface can be viewed as being significantly "softer", i.e., less resistant to distortion.

Figure 8b illustrates flow patterns for Re=1 when the liquid mass is reduced to D=0 and the interface is initially flat. The flow and deformation patterns remain qualitatively similar to the case with D=0.5 (compare Figs. 8a–b), with the velocity reduced due to the increased friction associated with the reduced liquid depth and the magnitude of the deformation increased due to the appearance of a larger pressure gradient. Further reduction of the mass of liquid to D=−0.5 leads to flow patterns displayed in Fig. 8c. They consist of two vortex cores surrounded by liquid flowing around them, as in the case of fixed contact points. As Ca increases, the intensity of the motion in the left core (on the hot side) noticeably decreases, primarily due to the increase of friction associated with the spatial constraint imposed by the location of the deforming interface.

The interplay between the available mass of the liquid (as measured by the bulge factor D) and the resulting interface deformation is illustrated in Fig. 3 displaying the maximum deformation as a function of Ca. The shape of the deformation curves clearly illustrates the formation of limit points for high enough values of Ca. The magnitude of the deformation in the case of the fixed contact angles is significantly larger and the range of permissible Ca's is significantly smaller as compared to the fixed contact points case. Increase of liquid mass from D=−0.5 to D=0.5 increases the range of permissible Ca's by a factor of more than three, but the maximum Ca that can be reached is only about 0.062, while it is almost 0.22 in the case of fixed contact points. It can be concluded that an increase of the liquid mass does provide significant opportunities for control of rupture in the case of wetting conditions leading to fixed contact angles, but the range of acceptable values of Ca is almost by an order of magnitude smaller than the one available in the fixed contact points case.

Figure 9 illustrates the evolution of the surface pressure and the shape of the interface as a function of Ca for three representative levels of liquid mass for Re=1. The shape of the interface is dominated by the contact angles. When D=0.5, the contact angles are positive and the distorted interface forms a bulge at the cold side (Fig. 9a). When D=0, the contact angles are zero and the interface can be described as rising at the cold end and forming a half-bulge there (Fig. 9b). When D=−0.5, interface moves up at the cold wall but without forming any bulge (Fig. 9c). Comparison of variations of pressure distributions as a function of D (see Figs. 9a−c) shows an increase of the pressure gradient in the core zone, an increase of the

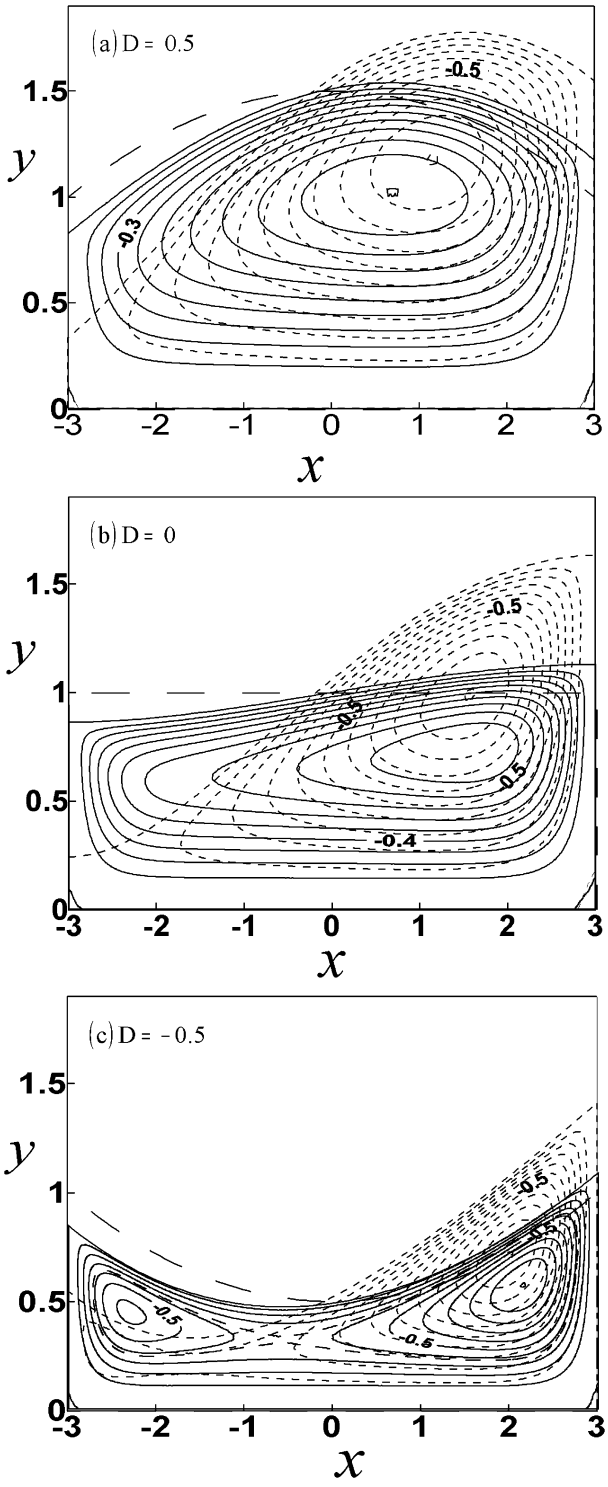

Fig. 8. Flow patterns for Re=1 and the interface subject to the fixed contact angles constraint. Contour lines are shown every 10% of ψ_{max}. Long-dash lines shows isothermal interface. Figure 8a–D=0.5: solid lines - Ca=0.02, $|\psi_{max}|$=0.0946; dash lines – Ca=0.06, $|\psi_{max}|$=0.1239. Figure 8b–D=0: solid lines - Ca=0.01, $|\psi_{max}|$=0.0437; dash lines – Ca=0.04, $|\psi_{max}|$=0.075. Figure 8c–D=-0.5: solid lines - Ca=0.005, $|\psi_{max}|$=0.0229; dash lines – Ca=0.015, $|\psi_{max}|$=0.0336.

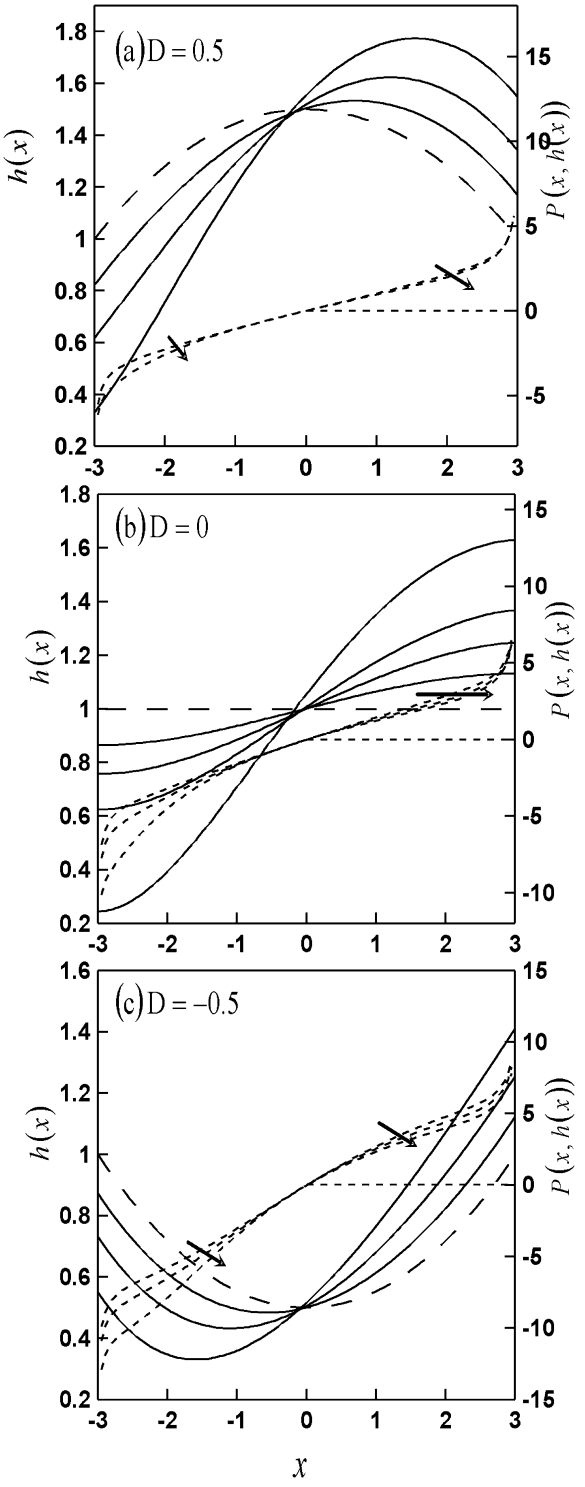

Fig. 9. The evolution of the surface pressure and the shape of the interface as a function of capillary number Ca for Re=1 and the interface subject to the fixed contact angles constraint. Figure 9a–D=0.5 (interface shown for Ca=0.02, 0.04, 0.06; pressure shown for Ca=0.02, 0.06); Figure 9b–D=0 (interface shown for Ca=0.01, 0.02, 0.03, 0.04; pressure shown for Ca=0.01, 0.03, 0.04); Figure 9c –D= -0.5 (interface and pressure shown for Ca=0.005, 0.01, 0.015). The long-dash line shows isothermal interface. The top dash line always corresponds to the pressure with the lowest Ca.

lengths of the turning zones and an increase of the differences between the turning zones for higher values of Ca as the mass of the liquid is reduced. All these effects are associated with the increase of friction due to the reduced depth of the liquid, similarly as has already been discussed in the case of fixed contact points (see Section 3.1.1).

Change in the flow pattern resulting from an increase of Reynolds number to Re=400 is illustrated in Fig. 10a for D=0.5 and two extreme values of capillary number Ca=0.02 and Ca=0.14. The flow pattern remains qualitatively similar to the case of Re=1 (compare Figs. 8a and 10a). The deformation pattern acquires new characteristics associated with the stronger vortex effects, similarly as in the case of fixed contact points (compare Figs. 5a and 10a). The new features include a "dip" in the interface above the vortex, and a small bulge forming at the cold wall. The form of the deformation suggest that the rupture may occur either through the formation of a dry spot at the cavity bottom at the hot end or through some form of breakdown driven by the local system dynamics at the cold contact point. The reduction of the mass of the liquid to D=0 (Fig. 10b) and then to D=−0.5 (Fig. 10c) reduces the magnitude of the deformation, reduces the intensity of the vortex and eliminates the "dip" from the interface. The evolution of the system response is qualitatively similar as in the case of fixed contact points and its description will not be repeated.

The relation between the quantity of the liquid and the interface deformation at Re=400 is illustrated in Fig. 6 displaying variations of the maximum deformation as a function of Ca. The formation of the limit points as well as an increase of the permissible values of Ca by a factor of around six due to the increase of the liquid mass from D=−0.5 to D=0.5 are clearly visible. The overall reduction of the permissible values of Ca associated with the relaxation of the interface constraints from the fixed contact points case to the fixed contact angles case is also visible. Increase of the mass of the liquid offers a better potential for rupture control at this value of Re as compared to Re=1 (compare Figs. 3 and 6).

Figure 11 illustrates the evolution of the surface pressure and the shape of the interface as a function of Ca at Reynolds number Re=400. The shape of the interface remains dominated by the contact angles similarly as for Re=1 (compare Figs. 9 and 11). Comparison of variations of pressure distributions as a function of the amount of liquid (see Figs. 11a–c) shows an increase of the pressure gradient in the core zone, an increase of the lengths of the turning zones and an increase of the differences between the turning zones for higher values of Ca as the mass of the liquid is reduced, similarly as in the case of Re=1 (compare Figs. 9 and 11). All these effects are associated with the increase of the friction due to the reduced depth of the liquid, as discussed previously.

4. CONCLUSIONS

We have investigated Marangoni convection in a cavity that is initially either over-filled or only partially filled with the liquid. The total mass of the liquid changes depending on the level of cavity over-fill. The liquid is heated and the resulting steady-state flow and deformation patterns are determined numerically by solving the complete governing equations including the complete deformation effects. The initial form of the contact conditions is maintained during the heating. Two cases of contact conditions are considered. In the first one, the contact points are fixed during the heating, and in the second one the contact angles are fixed and the liquid is permitted to move along the sidewalls. Detailed results are presented for the case of conduction limit (Marangoni number Ma→ 0), Biot number Bi→ (very high heat transfer coefficient at the interface) and the cavity length L=6.

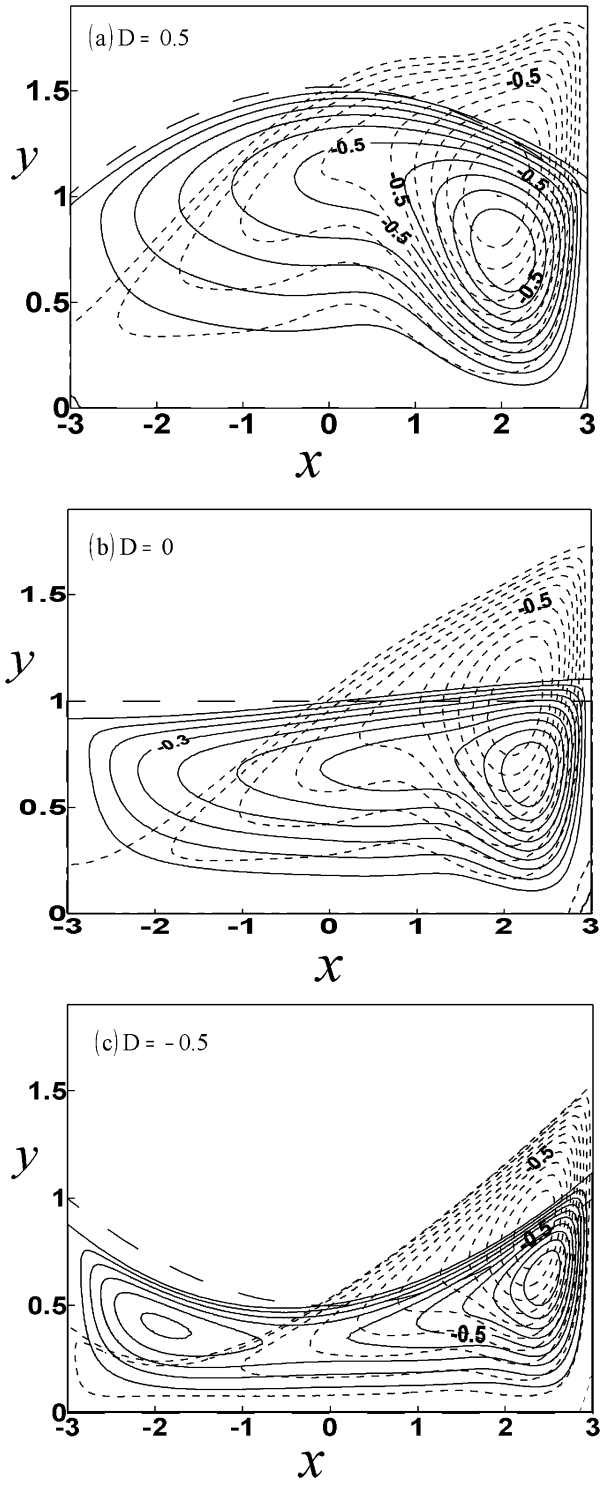

Fig. 10. Flow patterns for Re=400 and the interface subject to the fixed contact angles constraint. Contour lines are shown every 10% of ψ_{max}. Long-dash lines shows isothermal interface. Figure 10a–D=0.5: solid lines - Ca=0.02, $|\psi_{max}|$=0.0689; dash lines – Ca=0.14, $|\psi_{max}|$=0.0752. Figure 10b–D=0: solid lines - Ca=0.01, $|\psi_{max}|$=0.0454; dash lines – Ca=0.06, $|\psi_{max}|$=0.0575. Figure 10c–D =-0.5: solid lines - Ca=0.005, $|\psi_{max}|$=0.0226; dash lines – Ca=0.02, $|\psi_{max}|$=0.0335.

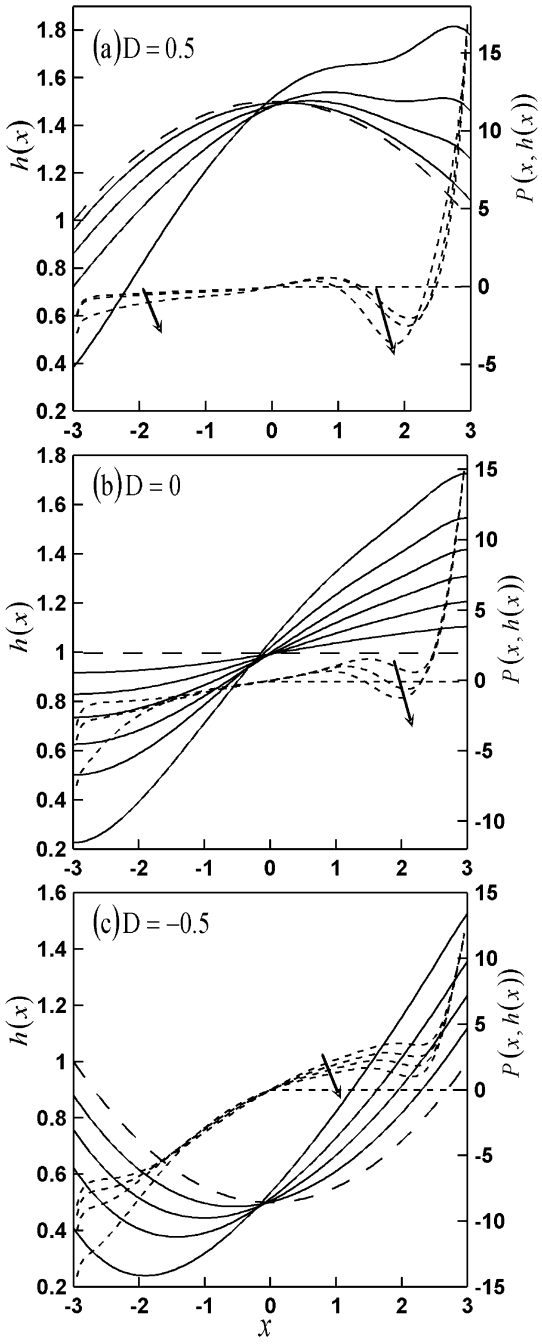

Fig. 11. The evolution of the surface pressure and the shape of the interface as a function of capillary number Ca for Re=400 and the interface subject to the fixed contact angles constraint. Figure 11a– D=0.5 (interface shown for Ca=0.02, 0.06, 0.1, 0.14; pressure shown for Ca=0.02, 0.06, 0.14); Figure 11b–D=0 (interface shown for Ca= 0.01, 0.02, 0.003, 0.04, 0.05, 0.06; pressure shown for Ca= 0.01, 0.04, 0.06), Figure 11c –D=-0.5 (interface and pressure shown for Ca=0.005, 0.01, 0.015, 0.02). The long-dash line shows isothermal interface. The top dash line always corresponds to the pressure with the lowest Ca.

The results show that steady convection and continuous interface exist only for a certain range of capillary numbers Ca. When Ca approaches its critical value Ca_{cr} (limit point), the magnitude of the deformation increases rapidly. The shape of the interface implies initiation of a process leading to interface rupture, with the form of potential rupture changing significantly depending on the flow conditions and type of heating.

When the interface is subject to the fixed contact points constraint, the rupture will most likely involve formation of a dry spot at the hot wall. When Re is high enough and the cavity is sufficiently over-filled, the rupture will most likely be driven by the dynamics of the cold contact point. When the fixed contact angles condition is imposed, the rupture will most likely involve formation of a dry spot at the cavity bottom at the hot end, unless Re and mass of the liquid are high enough for the dynamics of the cold contact point to dominate. When Re is high enough and the liquid is sufficiently deep, the rupture may involve some form of breakdown around the contact points regardless of the form of the contact constraint.

The convection pattern associated with heating through the sidewalls consists in general of a single dominant vortex driven along the interface from the hot to the cold end and the return flow driven by the longitudinal pressure gradient. When the cavity is only partially filled, this pattern is characterized by the appearance of two vortex cores. The deformation pattern is dominated by the pressure gradient; such pressure distribution causes the interface to rise at the cold side and recede at the hot side. This general pattern is changed for high enough Re and large enough mass of the liquid, which permit the formation of a strong vortex core with inviscid characteristics. The associated change in the pressure distribution generates a ''dip'' in the shape of the interface above the vortex core. This ''vortex effect'' can be sufficiently strong to reverse the deformation pattern and cause the fluid to rise at the hot end. In general, relaxation of the contact conditions from the fixed contact points constraints to the fixed contact angles constraints significantly increase the magnitude of the deformation and reduces the permitted range of capillary numbers.

It is demonstrated that an increase of the cavity over-fill leads to an increase of the critical value of capillary number Ca_{cr} and in this sense it delays the onset of rupture. Ca_{cr} doubles when the bulge factor changes from $D=-0.5$ to $D=0.5$ for $Re=1$ and triples for $Re=400$. The same factor increases from around three to almost six when contact angles are fixed. The relative change is thus much bigger in the fixed angles case, but the absolute change is nevertheless much smaller. When fixed contact angles are replaced by fixed contact points, change of D from $D=-0.5$ to $D=0$ increases Ca_{cr} by a factor of three, but further change of D to $D=0.5$ increases Ca_{cr} by only 20%.

If the interface rupture presents a concern in a given application, the present results suggests that at first one should attempt to fix the location of the end points of the interface, and then start adding liquid to the cavity.

ACKNOWLEDGMENT

This work was supported by the NSERC of Canada. Computing resources have been provided by SHARCNET.

REFERENCES

1. Kuhlmann, H.C., ''Thermocapillary convection in models of crystal growth,'' *Springer Tracts in Modern Physics, Springer Berlin Heidelberg*, Vol. 152, 1999.

2. Neitzel, G.P. and Dell'Aversana, P., "Noncoalescence and nonwetting behaviour of liquids," *Annual Review of Fluid Mechanic*, Vol. 34, pp. 267–289, 2002.
3. Schatz, M.F. and Neitzel, G.P., "Experiments in thermocapillary instabilities," *Annual Review of Fluid Mechanic*, Vol. 33, pp. 93–127, 2001.
4. Davis, S.H., "Thermocapillary instabilities," *Annual Review of Fluid Mechanic*, Vol. 19, pp. 403–435, 1987.
5. Ostrach, S., "Low gravity fluid flows," *Annual Review of Fluid Mechanic*, Vol. 14, pp. 313–345, 1982.
6. Floryan, J.M. and Chen, C., "Thermocapillary convection and existence of continuous liquid layers in the absence of gravity," *Journal of Fluid Mechanics*, Vol. 277, pp. 303–329, 1994.
7. Scriven, L.E. and Sterling, C.V., "The marangoni effect," *Nature*, Vol. 187, pp. 186–188, 1960.
8. Pearson, J.R.A., "On convection cells induced by surface tension," *Journal of Fluid Mechanics*, Vol. 4, pp. 489–500, 1958.
9. Czechowski, L. and Floryan, J.M., "Marangoni instability in a finite container – transition between short and long wavelengths modes," *ASME Journal of Heat Transfer*, Vol. 123, pp. 96–104, 2001.
10. Berdnikov, V.S., Gaponov, V.A. and Kovrizhnykh, L.S., "Thermal gravitational-capillary convection in a cavity with a longitudinal temperature gradient," *Journal of Engineering Phys. and Thermophysics*, Vol. 74, pp. 999–1006, 2001.
11. Kurosawa, T., Ueno, I. and Kawamura, H., *Journal of The Japan Society of Microgravity Application*, Vol. 18 (Suppl), pp. 45–46, 2001.
12. Sen, A.K. and Davis, S.H., "Steady thermocapillary flows in two-dimensional slots," *Journal of Fluid Mechanics*, Vol. 121, pp. 163–186, 1982.
13. Laure, P., Roux, B. and Ben Hadid, H., "Non-linear study of the flow in a long rectangular cavity subjected to thermocapillary effect," *Physics of Fluids A*, Vol. 2, pp. 516–524, 1990.
14. Ben Hadid, H. and Roux, B., "Buoyancy and thermocapillary driven flows in differentially heated cavities for low prandtl number fluids," *Journal of Fluid Mechanics*, Vol. 235, pp. 1–36, 1991.
15. Canright, D. and Huber, M., "A boundary-layer model of thermocapillary flow in a cold corner," *Physics of Fluids*, Vol. 14, pp. 3272–3279, 2002.
16. Zebib, A., Homsy, G.M. and Meiburg, E., "High marangoni number convection in a square cavity," *Physics of Fluids*, Vol. 28, pp. 3467–3476, 1985.
17. Carpenter, B.M. and Homsy, G.M., "High marangoni number convection in a square cavity part II," *Physics of Fluids A*, Vol. 2, pp. 137–149, 1990.
18. Torii, S., "Unsteady thermal fluid transport phenomena in square cavity under reduced gravity," *International Journal of Computation Engineering Science*, Vol. 2, pp. 59–73, 2001.
19. Liu, Q.S., Roux, B. and Velarde, M.G., "Thermocapillary convection in two-layer systems," *International Journal of Heat Mass Transfer*, Vol. 41, pp. 1499–1511, 1998.
20. Braverman, L.M., Eckert, K., Nepomnyashchy, A.A., Simanovskii, I.B. and Thess, A., "Convection in two-layer system with anomalous thermocapillary effect," *Physics ReviewE.*, Vol. 62, pp. 3619–3631, 2000.
21. Peltier, L.J., Biringen, S., "Time-dependent thermocapillary convection in a rectangular cavity: numerical results for a moderate prandtl number fluid," *Journal of Fluid Mechanics*, Vol. 257, pp. 339–357, 1993.
22. Chen, J.C. and Hwu, F.S., "Oscillatory thermocapillary flow in a rectangular cavity," *International Journal of Heat Mass Transfer*, Vol. 36, pp. 3743–3749, 1993.
23. Hamed, M.S., Floryan, J.M., "Marangoni convection. Part 1. A cavity with differentially heated sidewalls," *Journal of Fluid Mechanics*, Vol. 405, pp. 79–110, 2000.

24. Jiang, Y., Badr, H. and Floryan, J.M., "Thermocapillary convection with moving contact points," *Physics of Fluids*, Vol. 15, pp. 442–454, 2003.
25. Jiang, Y. and Floryan, J.M., "Effect of heat transfer at the interface on the thermocapillary convection in the adjacent phase," *ASME Journal of Heat Transfer*, Vol. 125, pp. 190–194, 2003.
26. Benz, S. and Schwabe, D., "The three-dimensional stationary instability in dynamic thermocapillary shallow cavities," *Experiments of Fluids*, Vol. 31, pp. 409–416, 2001.
27. El-Gammal, M., Furmanski, P. and Floryan, J.M., 2003, "Thermocapillary convection in the over-filled and partially filled cavities," *Physics of Fluids*, Vol. 16, pp. 212–215, 2004.
28. Chen, C. and Floryan, J.M., "Numerical simulation of non-isothermal capillary interfaces," *Journal of Computational Physics*, Vol. 111, pp. 183–193, 1994.
29. Hamed, M. and Floryan, J.M., "Numerical simulation of unsteady nonisothermal capillary interfaces," *Journal of Computational Physics*, 145, pp. 110–140, 1998.
30. Moffat, H.K., "Viscous and resistive eddies near a sharp corner," *Journal of Fluid Mechanics*, 18, pp. 1–18, 1964.
31. Anderson, D.M. and Davis, S.H., "Local fluid and heat flow near contact lines," *Journal of Fluid Mechanics*, Vol. 268, pp. 231–265, 1994.
32. Batchelor, G.K., "On steady laminar flow with closed streamlines at large Reynolds numbers," *Journal of Fluid Mechanics*, Vol. 1, pp. 177–190, 1956.